Study of RgS^- and RgS (Rg = Ne, Ar, and Kr) via slow photoelectron velocity-map imaging spectroscopy and *ab initio* calculations

Etienne Garand[1,a)] and Daniel M. Neumark[1,2,b)]
[1]*Department of Chemistry, University of California, Berkeley, California 94720, USA*
[2]*Chemical Sciences Division, Lawrence Berkeley National Laboratory, Berkeley, California 94720, USA*

(Received 29 April 2011; accepted 8 June 2011; published online 8 July 2011)

High-resolution photoelectron spectra of RgS^- (Rg = Ne, Ar, and Kr) were obtained using slow electron velocity-map imaging (SEVI). The SEVI spectra reveal well-resolved vibrational transitions between multiple spin-orbit states of RgS^- and RgS, both of which are open-shell species. Detailed assignments are made by comparison with theoretical simulations based on high level *ab initio* calculations and a atoms-in-molecule model that accounts for spin-orbit coupling in the anion and neutral. Several RgS^- and RgS vibrational frequencies and excited-state term energies are accurately determined from the analysis of the experimental spectra and are found to be in excellent agreement with the calculated values. © *2011 American Institute of Physics*. [doi:10.1063/1.3605595]

I. INTRODUCTION

The interatomic and intermolecular forces induced by non-covalent interactions play a key role in many fields of chemistry and biology.[1,2] These long-range interactions include dispersion, induction, and hydrogen-bonding, and they drive diverse phenomena ranging from protein-ligand recognition[3] to cold molecule collision dynamics.[4] The study of isolated neutral[5–7] and ionic[8] clusters provides an elegant means for studying non-covalent interactions, since the structure, spectroscopy, and dynamics of these species often reflect the interplay among multiple and competing long-range forces.

Clusters comprising open-shell atoms or molecules pose a particular challenge to both theory and experiment because multiple close-lying electronic states associated with the open-shell species are typically coupled and split within the cluster.[9,10] Potential energy curves for the simplest of such species, diatomic complexes comprising a rare gas and an open shell atom, were originally obtained from scattering experiments.[11–14] Photodetachment of the corresponding diatomic anion has also proved to be a powerful spectroscopic probe of both the anionic and neutral electronic and vibrational levels of these systems.[15] However, high resolution is required in order to resolve the low-frequency vibrations that are characteristic of these species. In the first series of experiments of this type, anion zero electron kinetic energy (ZEKE) spectroscopy[16] was applied to the study of rare gas halide complexes.[17–20] The recently developed slow electron velocity map imaging (SEVI) method,[21,22] which offers comparable resolution (as high as 2–3 cm^{-1}) but is experimentally easier to implement, has been used to study van der Waals interactions in the ClH_2,[23] ArO,[24] and KrO[25] complexes. The spectroscopic information obtained from the anion ZEKE and SEVI experiments complements scattering experiments on the neutral systems and ion mobility studies[26,27] on the anions.

Here, we expand our investigation of weakly bound open shell systems by measuring SEVI spectra of rare gas sulfide anions, RgS^-, with Rg = Ne, Ar, and Kr. Both the anionic and neutral RgS species are open-shell complexes, as is the case for the isovalent RgO complexes that were initially studied by Bowen and co-workers.[28] As a result, the SEVI spectra yield information on the electronic structure and spin-orbit couplings in both the anionic and neutral complexes. However, the RgS complexes are expected to have shallower well depths and larger spin-orbit interactions than the RgO species,[14,29] potentially leading to qualitatively different electronic and vibrational structure in the SEVI spectra.

There is considerably less information on rare gas-sulfur complexes compared to O and O^-. The interaction potentials between rare gases and neutral sulfur atoms have been previously obtained from molecular beam scattering experiments and theoretical calculations.[29–31] Aquilanti *et al.*[29] found that while the experimental glory structure of S-Ne could be fitted by using just the spherical component of the potential, scattering experiments involving heavier rare gas atoms resulted in glory patterns that were quenched in amplitude and whose extrema were shifted in energy when compared to those predicted by isotropic interactions alone. The experimental results showed that going from Ne to Xe, the anisotropic component of the potential played an increasingly important role, indicative of bond stabilization via charge transfer between the sulfur and the rare gas atoms. On the theoretical side, Klos *et al.*[30] calculated the interaction potentials of Rg-S(^3P) in $^3\Pi$ and $^3\Sigma^-$ states using unrestricted CCSD(T) and extended correlation consistent basis sets augmented by bond functions. The only reported results on Rg/S^- interactions come from a theoretical study of HeS^-.[32]

a)Present address: Sterling Chemistry Laboratory, Yale University, P.O. Box 208107, New Haven, Connecticut 06520, USA.
b)Author to whom correspondence should be addressed: Electronic mail: dneumark@berkeley.edu.

In this paper, we present high-resolution photoelectron spectra of RgS^- (Rg = Ne, Ar, and Kr) obtained using SEVI. The NeS^- results represent the first observation and characterization of an anionic Ne complex. Numerous well-resolved transitions are observed for each species, and show an increasing perturbation of the fine-structure associated with S^- photodetachment with increasing mass of the Rg atom. New interaction potentials for the RgS anion and neutral complexes are calculated based on an advanced *ab initio* level of theory and a atoms-in-molecule model of the spin-orbit coupling. These potentials allow us to simulate the SEVI spectrum with high accuracy and to assign its resolved features. Several spectroscopic constants determined from analysis of the experimental spectra are found to be in excellent agreement with the calculated values.

II. EXPERIMENTAL SECTION

The SEVI apparatus has been described in detail in Refs. 21 and 22. SEVI is a high resolution variant of photoelectron spectroscopy based on photoelectron imaging, in which mass-selected anions are photodetached at a series of wavelengths. The resulting photoelectrons are collected by velocity-map imaging (VMI) (Ref. 33) using relatively low extraction voltages, with the goal of selectively detecting slow electrons with high efficiency and enlarging the corresponding image on the detector. At each wavelength, a high resolution photoelectron spectrum is obtained over a limited range of electron kinetic energy (eKE).

The NeS^- and ArS^- anions were produced from a gas mixture comprising 0.1% of CS_2 in a balance of neon or argon. Similarly, the KrS^- anions were produced from a gas mixture comprising 0.1% CS_2 and 15% of krypton in a balance of argon. The gas mixture, at a stagnation pressure of 350 psi, was expanded into the source vacuum chamber through an Even-Lavie pulsed valve[34] equipped with a circular ionizer. The anions were perpendicularly extracted into a Wiley-McLaren time-of-flight mass spectrometer[35] and directed to the detachment region by a series of electrostatic lenses and pinholes. A pulsed voltage on the last ion deflector allowed only the desired mass into the interaction region. Anions were photodetached between the repeller and the extraction plates of the VMI stack by the gently focused output of a Nd:YAG-pumped tunable dye laser. The photoelectron cloud formed was coaxially extracted down a 50 cm flight tube and mapped onto a detector comprising a chevron-mounted pair of time-gated, image-quality microchannel plates coupled to a phosphor screen, as is typically used in photofragment imaging experiments.[36] Events on the screen were collected by a 1024×1024 pixels charge-coupled device camera and sent to a computer. Electron velocity-mapped images resulting from 30 000–50 000 laser pulses were summed, quadrant symmetrized, and inverse-Abel transformed. Photoelectron spectra were obtained via angular integration of the transformed images. The spectra presented here are plotted with respect to electron binding energy (eBE), defined as the difference between the energy of the photodetachment photon and the measured eKE.

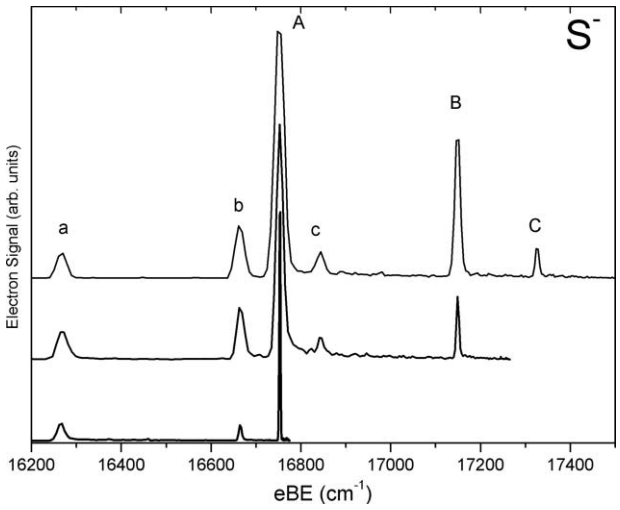

FIG. 1. The SEVI spectra of atomic S^-, acquired at photon energies of 17 537 cm^{-1}, 17 265 cm^{-1}, and 16 774 cm^{-1}. The traces are offset for clarity.

III. EXPERIMENTAL RESULTS

For reference and calibration, SEVI spectra of atomic S^-, acquired at photon energies of 17 537 cm^{-1}, 17 265 cm^{-1}, and 16 774 cm^{-1}, are shown in Fig. 1. In SEVI, all observed transitions within the same image have similar widths in pixels (Δr), which means transitions observed further from threshold (larger r) are broader in energy. With the −350 V VMI repeller voltage used in this study, the full width at half-maximum Γ for each transition as a function of eKE was found to fit a quadratic expression,

$$\Gamma = 2.0 + 0.034(\text{eKE}) - 1.4 \times 10^{-6}(\text{eKE})^2, \quad (1)$$

where the units are in wavenumbers.

Six features are clearly seen in the spectra in Fig. 1. They can readily be assigned to the six spin-orbit transitions of atomic sulfur. Features A, B, and C originate from the photodetachment of the anion $^2P_{3/2}$ state to the neutral $^3P_2$, $^3P_1$, and $^3P_0$ states, respectively. Feature A, at 16 753 cm^{-1}, corresponds to the origin transition and yields the electron affinity of atomic sulfur, in accordance with the previously determined value of 16 752.976 cm^{-1}.[37] The 396 cm^{-1} and 573 cm^{-1} shifts from origin of features B and C, respectively, thus correspond to the spin-orbit splitting of the ^3P states. These are in excellent agreement with the previously determined values of 396.055 cm^{-1} and 573.640 cm^{-1}.[38] The weaker features a, b, and c are from photodetachment of the anion $^2P_{1/2}$ excited spin-orbit state to the neutral $^3P_2$, $^3P_1$, and $^3P_0$ states, respectively. Feature a, when compared to the origin transition, yields the anion spin-orbit splitting of 484 cm^{-1}, again in agreement with the previously determined value of 483.54 cm^{-1}.[39] The values of the transitions from Fig. 1 are listed in Table I.

The composite SEVI spectrum of NeS^-, acquired at photon energies of 17 537 cm^{-1}, 17 295 cm^{-1}, and 16 831 cm^{-1} is shown in Fig. 2. The highest resolution parts of each trace were stitched together at baseline points and the peak intensities were normalized to those of the trace taken at the highest photon energy. This is the first reported spectrum of an

TABLE I. Experimental peak positions, shift from origin, and assignments of the S^- SEVI spectra. Estimated error bars for peaks A–C are ±2 cm^{-1}.

Peak	Position (cm^{-1})	Shift from origin (cm^{-1})	Assignment
a	16 266	−487	$^3P_2 \leftarrow {}^2P_{1/2}$
b	16 665	−88	$^3P_1 \leftarrow {}^2P_{1/2}$
A	16 753	0	$^3P_2 \leftarrow {}^2P_{3/2}$
c	16 843	90	$^3P_0 \leftarrow {}^2P_{1/2}$
B	17 149	396	$^3P_1 \leftarrow {}^2P_{3/2}$
C	17 326	573	$^3P_0 \leftarrow {}^2P_{3/2}$

anionic neon cluster. The overall appearance of the spectra is very similar to the atomic S^- spectrum, shown as a dashed line in Fig. 2. The intensities of the features in the NeS^- spectra are comparable to the S^- spectrum, but the positions of all the features are blueshifted by ∼45 cm^{-1}. Furthermore, the most intense feature in the NeS^- spectrum is split into two closely spaced peaks, labeled A and B and separated by 9 cm^{-1}. Table II lists the peak positions of the observed features in Fig. 2.

The composite SEVI spectrum of ArS^-, acquired at photon energies of 17 849 cm^{-1}, 17 506 cm^{-1}, 17 147 cm^{-1}, and 17 060 cm^{-1}, is shown in Fig. 3. In contrast to the NeS^- spectrum, the ArS^- spectrum displays clear differences when compared to atomic S^-. In particular, a well separated peak progression starting at 17 042 cm^{-1} with a peak separation of ∼25 cm^{-1}, labeled A–D, is clearly visible and constitutes the most intense features of the spectrum. The other intense feature of the spectrum, labeled E, appears at 17 437 cm^{-1}, and is shifted by 395 cm^{-1} from feature A. In contrast to the S^- and NeS^- spectra, the ArS^- spectrum does not exhibit any features that are significantly redshifted from the most intense features. The very weak features a and b are redshifted by only 13 cm^{-1} and 27 cm^{-1} from peak A. Table III lists the peak positions of the features observed in Fig. 3.

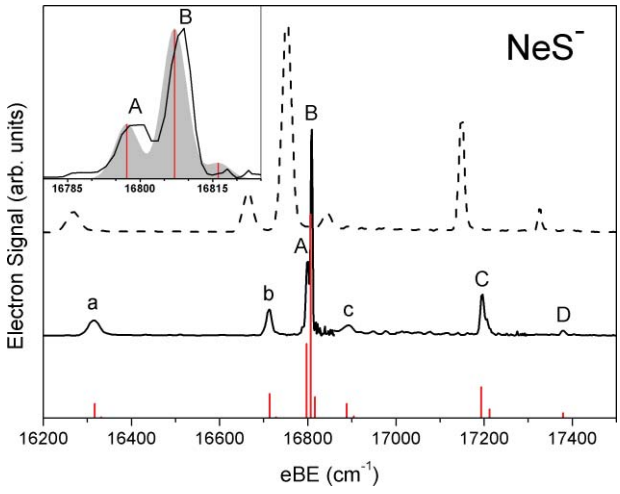

FIG. 2. The composite experimental SEVI spectrum of NeS^- (black trace), acquired at photon energies of 17 537 cm^{-1}, 17 295 cm^{-1}, and 16 831 cm^{-1} and the Franck-Condon simulations (red vertical lines). The SEVI spectra of atomic S^-(dashed line) in shown for comparison. The inset shows an expanded view of the peaks A and B. Solid grey features represent a convolution of the FC simulation with the experimental resolution.

TABLE II. Experimental and calculated peak positions and shift from origin along with transition assignments of the NeS^- SEVI spectrum. Estimated error bars for peaks A–D are ±5 cm^{-1}.

Peak	Position (cm^{-1})	Shift from origin (cm^{-1})	Calculated position (cm^{-1})	Assignment
a	16 315	−484	16 316.5	*X*2,0 ← *II*,0
b	16 712	−87	16 713.1	*II*0,0 ← *II*,0
A	16 799	0	16 797.3	*X*2,0 ← *X*,0
B	16 808	9	16 807.1	*I*1,0 ← *X*,0
c	16 890	91	16 888.4	*III*0,0 ← *II*,0
C	17 194	395	17 193.3	*II*0,0 ← *X*,0
D	17 379	580	17 379.0	*III*0,0 ← *X*,0

The composite SEVI spectrum of KrS^-, acquired at photon energies of 17 945 cm^{-1}, 17 692 cm^{-1}, 17 385 cm^{-1}, and 17 250 cm^{-1} is shown in Fig. 4. The KrS^- spectrum shows an intense feature, labeled A, at 17 214 cm^{-1}. Blueshifted from feature A is a weaker peak progression, starting at 17 259 cm^{-1}, labeled B–F, with a peak separation of ∼20 cm^{-1}. Similar to ArS^-, the KrS^- spectrum shows a relatively intense feature, peak G, which is blueshifted by 396 cm^{-1} from peak A. Several weak features labeled a–e are observed at lower eBE than peak A. Table IV lists the peak positions of the features observed in Fig. 4.

The photoelectron images show that the photoelectron angular distributions for all the features in the S^- and RgS^- spectra in Figs. 1–4 are essentially isotropic, indicating almost pure *s-wave* detachment. This is similar to previously observed O^- and RgO^- SEVI spectra.[24,25]

IV. THEORY

Ab Initio calculations were performed with the MOLPRO 2009 suite of program[40] in order to aid in assigning the observed features in the RgS^- SEVI spectra. The electronic structure of the neutral[30] and anionic[32] RgS complexes as well as the isovalent RgO species[24,25,41–43] has

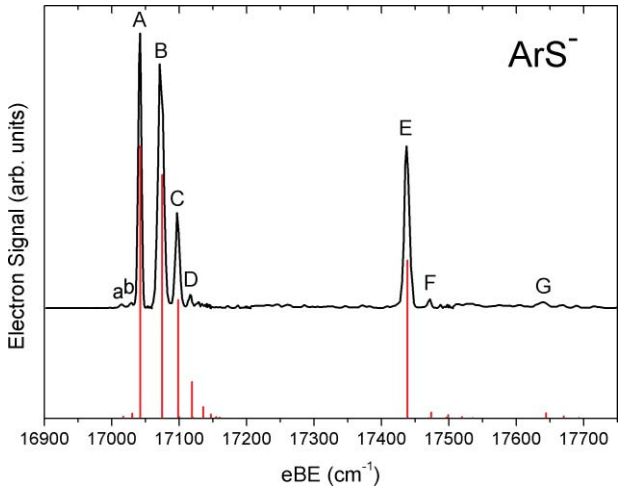

FIG. 3. The composite experimental SEVI spectrum of ArS^- (black trace), acquired at photon energies of 17 849 cm^{-1}, 17 506 cm^{-1}, 17 147 cm^{-1}, and 17 060 cm^{-1} and the Franck-Condon simulation (red vertical lines).

TABLE III. Experimental and calculated peak positions and shift from origin along with transition assignments of the ArS^- SEVI spectrum. Estimated error bars for peaks A–G are ±5 cm^{-1}.

Peak	Position (cm^{-1})	Shift from origin (cm^{-1})	Calculated position (cm^{-1})	Assignment
a	17 015	−27	17 015.2	$X2,0 \leftarrow I,0$
b	17 029	−13	17 030.6	$X2,1 \leftarrow X,1$
A	17 042	0	17 042.5	$X2,0 \leftarrow X,0$
B	17 073	31	17 074.7	$I1,0 \leftarrow X,0$
C	17 097	55	17 098.7	$I1,1 \leftarrow X,0$
D	17 116	74	17 119.1	$I1,2 \leftarrow X,0$
E	17 437	395	17 438.5	$II0,0 \leftarrow X,0$
F	17 471	429	17 473.8	$II1,0 \leftarrow X,0$
G	17 640	598	17 644.2	$III0,0 \leftarrow X,0$

been discussed in detail previously. Briefly, the interaction of a $S^-(^2P)$ atom with a rare gas atom gives rise to a $^2\Sigma^+$ state and a $^2\Pi$ state. In terms of the atomic orbitals of S^-, the electronic configuration of these two states can be described as $p_x^2 p_y^2 p_z^1$ and $p_x^1 p_y^2 p_z^2$, respectively, where the z axis is oriented along the molecular axis. Similarly, a neutral $S(^3P)$ atom interacting with a rare gas atom gives rise to a $^3\Pi$ state ($p_x^2 p_y^1 p_z^1$) and a $^3\Sigma^-$ state ($p_x^1 p_y^1 p_z^2$).

The NeS and ArS anion and neutral potentials, for interatomic distances between 2.4 Å and 20 Å, were first calculated at the restricted coupled cluster level of theory with singles, doubles, and perturbative triples level,[44,45] keeping the core electrons frozen (FC-RCCSD(T)). The augmented correlation consistent polarized valence basis sets,[46] aug-cc-pV*N*Z with $N = Q(4)$, 5, and 6, (hereafter denoted as AV*N*Z) were used for both the sulfur and rare gas atoms. All interaction energies were corrected for basis set superposition error using the counterpoise procedure of Boys and Bernardi.[47] The calculated energies at every internuclear distance were then extrapolated to the complete basis set (CBS) limit[48] by separately fitting the Hartree-Fock (E_{HF}) and coupled-cluster

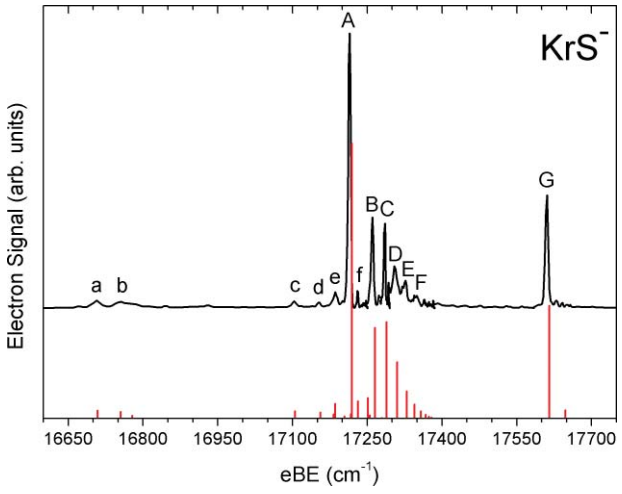

FIG. 4. The composite experimental SEVI spectrum of KrS^- (black trace), acquired at photon energies of 17 945 cm^{-1}, 17 692 cm^{-1}, 17 385 cm^{-1}, and 17 250 cm^{-1} and the Franck-Condon simulation (red vertical lines).

TABLE IV. Experimental and calculated peak positions and shift from origin along with transition assignments of the KrS^- SEVI spectrum. Estimated error bars for peaks A–G are ±5 cm^{-1}.

Peak	Position (cm^{-1})	Shift from origin (cm^{-1})	Calculated position (cm^{-1})	Assignment
a	16 707	−507	16 709.1	$X2,0 \leftarrow II,0$
b	16 756	−458	16 754.9	$I1,0 \leftarrow II,0$
c	17 103	−111	17 105.2	$II0,0 \leftarrow II,0$
d	17 153	−61	17 154.1	$II1,0 \leftarrow II,0$
e	17 186	−28	17 185.4	$X2,0 \leftarrow I,0$
A	17 214	0	17 219.5	$X2,0 \leftarrow X,0$
f	17 231	17	17 231.2	$I1,0 \leftarrow I,0$
B	17 259	45	17 265.2	$I1,0 \leftarrow X,0$
C	17 284	70	17 288.9	$I1,1 \leftarrow X,0$
D	17 305	91	17 310.1	$I1,2 \leftarrow X,0$
E	17 324	110	17 329.1	$I1,3 \leftarrow X,0$
F	17 347	133	17 345.0	$I1,4 \leftarrow X,0$
G	17 610	396	17 615.5	$II0,0 \leftarrow X,0$

(E_{CC}) energies as a function of the basis set parameter N with

$$E_{HF}(N) = E_{HF}^{CBS} + A \times \exp(-B \times N), \quad (2)$$

$$E_{CC}(N) = E_{HF}^{CBS} + (C \times N^{-3}), \quad (3)$$

where *A*, *B*, and *C* are fitting parameters. Three points (N = Q, 5, and 6) were used for the Hartree-Fock energy extrapolation while only two (N = 5 and 6) were used for the coupled-cluster energy.[48] The core correlation and nonrelativistic effects were calculated by correlating all electrons (AE-RCCSD(T)) in conjunction with the second-order Douglas–Kroll (DK) Hamiltonian[49–51] and using the relativistic augmented correlation consistent polarized core-weighted valence basis set with quadruple zeta (ApwCVQZ-DK).[52] The final potentials, denoted AE-CCSD(T)/CBS-DK, were constructed by adding the difference between the AE-RCCSD(T)/ApwCVQZ-DK and the FC-RCCSD(T)/AVQZ energies to the complete basis set extrapolated energies. The KrS anion and neutral potentials were calculated in a similar manner but in order to better account for the more important relativistic effects, the FC-RCCSD(T)/

TABLE V. Parameters of the spin-orbit coupled potentials of the NeS anion and neutral calculated using the *ab initio* AE-RCCSD(T)/CBS-DK potentials. Note that ν is the fundamental (not the harmonic) vibrational frequency.

	R_e (Å)	D_e (cm^{-1})	T_0 (cm^{-1})	D_0 (cm^{-1})	ν (cm^{-1})
			NeS^-		
X	3.897	91.4	0	78.7	21.4
I	4.148	79.9	10.1	68.7	19.4
II	4.045	83.7	490.6	71.7	20.2
			NeS		
*X*2	3.596	47.1	0	34.5	18.9
*I*1	3.829	34.9	9.8	24.6	14.5
*I*0	3.892	32.7	11.6	22.8	13.8
*II*0	3.596	47.1	396.1	34.5	18.9
*II*1	3.843	34.6	406.4	24.1	14.5
*III*0	3.776	37.4	581.7	26.4	15.5

TABLE VI. Parameters of the spin-orbit coupled potentials of the ArS anion and neutral calculated using the *ab initio* AE-RCCSD(T)/CBS-DK potentials.

	R (Å)	D_e (cm^{-1})	T_0 (cm^{-1})	D_0 (cm^{-1})	ν (cm^{-1})
			ArS$^-$		
X	3.744	431.4	0	409.1	43.5
I	3.955	404.2	27.3	381.8	40.9
II	3.881	412.1	504.2	388.4	43.9
			ArS		
*X*2	3.722	137.1	0	119.7	31.6
*I*1	3.963	101.1	32.3	87.4	24.0
*I*0	4.041	95.3	38.4	81.3	24.2
*II*0	3.721	137.1	396.1	119.7	31.6
*II*1	3.998	99.5	431.4	84.4	25.4
*III*0	3.927	107.2	601.8	91.5	26.5

AVNZ-DK with N = T, Q, 5 energies were used for the CBS extrapolation.

The resulting NeS, ArS, and KrS anion and neutral potentials are presented in Tables S1–S3 of the supplementary material.[53] The potential well depth (D_e) and equilibrium bond distance (R_e) were obtained by fitting the calculated energy points with a 7th order Murrell-Sorbie potential,[54]

$$V(R) = -D_e\left[1 + \sum_{i=1}^{7} a_i(R - R_e)^i\right]\exp\left(a_1(R - R_e)\right), \quad (4)$$

where a_i are adjustable parameters. The fitting parameters for the all the AE-CCSD(T)/CBS-DK potential energy curves are presented in Tables S4–S6 of the supplementary material.[53] The calculated potentials for anionic NeS$^-$, ArS$^-$, and KrS$^-$ are reported for the first time. However, their neutral counterparts can be compared to the previously reported calculations of Klos *et al.*[30] For NeS, the present calculated values of D_e and R_e are very close to those previously reported at the FC(1s)-UCCSD[T] level using the AV5Z basis set augmented with 3*s*3*p*2*d*2*f*1*g* mid-bond functions (AV5Z+33221). For ArS and KrS, our calculations yield potential wells, which are deeper by 4–11 cm^{-1} than the previous FC-UCCSD(T)/AVQZ+332 calculations. Our calculated values of D_e and R_e are also within the error bars of the potentials derived by Aquilanti *et al.*[29] from scattering experiments.

TABLE VII. Parameters of the spin-orbit coupled potentials of the KrS anion and neutral calculated using the *ab initio* AE-RCCSD(T)/CBS-DK potentials.

	R_e (Å)	D_e (cm^{-1})	T_0 (cm^{-1})	D_0 (cm^{-1})	ν (cm^{-1})
			KrS-		
X	3.726	653.2	0	629.9	46.2
I	3.936	620.1	34.1	595.8	45.0
II	3.869	628.6	510.3	603.1	49.1
			KrS		
*X*2	3.781	180.5	0	163.4	32.1
*I*1	4.027	130.7	45.7	117.7	23.7
*I*0	4.128	121.7	54.9	108.5	24.4
*II*0	3.781	180.5	396.1	163.4	32.1
*II*1	4.090	127.3	447.0	112.5	26.3
*III*0	4.012	137.9	614.8	122.3	27.2

Spin-orbit (SO) interaction further splits the molecular terms. For the neutral, there are six SO-coupled states designated as $n\Omega(j)$: *X*2(2), *I*1(2), *I*0(2), *II*1(1), *II*0(1), and *III*0(0), where n indexes the states with the same projection Ω of the total electronic angular momentum j (with asymptotically good quantum number values of 0, 1, and 2) onto the molecular axis. Using similar $n^-\Omega^-(j^-)$ notation, the SO-coupled states of the anion are labeled *X*1/2(3/2), *I*3/2(3/2), and *II*1/2(1/2). For clarity, these electronic states will be denoted only as $n\Omega$ (*X*2, *I*1, *I*0, *II*1, *II*0, and *III*0) for the neutral and as n^- (*X*, *I*, and *II*) for the anion.

The potential energy curves including vectorial SO interaction were determined using the atoms-in-molecule model[14,41,55,56] that fixes the SO coupling constants at their asymptotic (atomic) values. Explicit expressions for the SO-coupled potentials arising from the interaction of a rare gas with ^{2}P and ^{3}P atoms have been given previously.[14] Asymptotic energies for separated atoms were set to experimental values. The asymptotic energies Δ_j of the terms correlating to Rg + S(^{3}P$_j$) limits referenced to the lowest j = 2 term are Δ_1 = 396.055 cm^{-1} and Δ_0 = 573.640 cm^{-1}. The Rg + S$^-$(^{3}P$_{1/2}$) limit lies Δ^- = 483.54 cm^{-1} above the ground Rg + S$^-$(^{3}P$_{3/2}$) limit. At the asymptote, the S$^-$(^{2}P$_{3/2}$) and S(^{3}P$_2$) are separated in energy by the electron affinity of atomic sulfur, EA = 16 752.972 cm^{-1}.

The SO coupled potentials are described in Tables V–VII and their Murrell-Sorbie fitting parameters are presented in Tables S7–S9 of the supplementary material.[53] The adiabatic transition energies T_0, dissociation energies D_0, and fundamental vibrational frequencies ν shown therein were obtained by solving the radial Schrödinger equations numerically for zero rotational angular momentum. Note that within the formalism used here, the potential energy curves for the neutral *X*2 and *II*0 states are identical;[57] the *II*0 state is shifted upward by 396 cm^{-1}, the spin-orbit splitting between the ^{3}P$_2$ and ^{3}P$_1$ levels of the S atom. The potential energy curves for NeS$^-$ and NeS are shown in Fig. 5.

Franck-Condon (FC) simulations were also performed in order to assign the observed spectra. Only bound-bound vibrational transitions were considered by using the vibrational wavefunctions from numerical solving of the radial Schrödinger equations. The relative photodetachment cross sections for the various different electronic transitions were left as adjustable parameters. The position of the peaks was calculated by using the experimental EA of S$^-$ as the asymptotic splitting between the anion and neutral ground states.

V. ANALYSIS

The results of the FC simulation are overlapped with the SEVI spectra of NeS$^-$, ArS$^-$, and KrS$^-$ in Figs. 2–4 respectively. The overall excellent agreement between the calculated FC spectra and the experimental spectra allows for unambiguous assignment of the SEVI spectral features. In the discussion below, notation such as *X*2,0 refers to the v = 0 vibrational level of the *X*2 state.

In the NeS$^-$ spectrum, feature A, at 16 799 cm^{-1}, is assigned to the *X*2,0 ← *X*,0 vibrational origin, in excellent agreement with the calculated value of 16 797.3 cm^{-1}. This

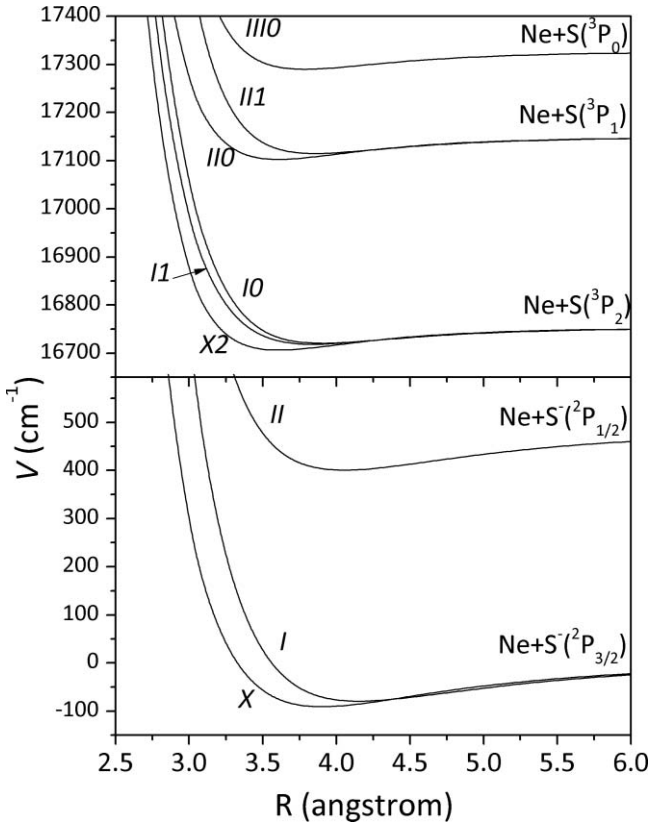

FIG. 5. Calculated spin-orbit coupled potential energy curves for NeS and NeS^-; parameters are given in Table V.

yields the EA of NeS to be 2.0828 ± 0.0006 eV. The more intense feature B, at 16 808 cm^{-1}, is assigned to the $I1,0 \leftarrow X$, 0 transition to the first excited spin-orbit state of the neutral NeS. The experimental $T_0(I1)$ of 9 ± 5 cm^{-1} agrees well with the calculated value of 9.8 cm^{-1}. Features C and D are assigned to the $II0,0 \leftarrow X,0$ and $III0,0 \leftarrow X,0$ transitions, respectively, giving the experimental values of $T_0(II0) = 395 \pm 5$ cm^{-1} and $T_0(III0) = 580 \pm 5$ cm^{-1}. These are again within 1 cm^{-1} of the calculated values. The intensity pattern of peaks A and B might suggest that peak B is the origin transition, while peak A is a hot band transition. However, this assignment would be inconsistent with the *II*0 term energy (peak C) which, as mentioned above, should be blueshifted from the *X*2 origin by 396 cm^{-1}. Moreover, since the *X*2 and *II*0 potential energy curves are the same, if peak A was a hot band, then peak C would appear as a doublet with the same intensity pattern as peaks A and B instead of as a sharp isolated feature. Peaks a, b, and c all originate from the ground vibrational state of the second spin-orbit excited state *II*,0 of the NeS^- anion. They are assigned to the transitions $X2,0 \leftarrow II,0$, $II0,0 \leftarrow II,0$, and $III0,0 \leftarrow II,0$, respectively. Thus, the anionic term value $T_0(II)$ is 484 ± 5 cm^{-1}. No features originating from the anion first excited state (*I*) are observed in the SEVI spectrum of NeS^- even though the second excited state (*II*) is clearly populated. This situation may reflect a low photodetachment cross section out of the *I* state, or a higher than thermal population in the *II* state owing to the spin-flip transition required to quench it in the free jet expansion.

In the ArS^- spectrum, feature A at 17 042 cm^{-1} is assigned to the origin $X2,0 \leftarrow X,0$ transition, in excellent agreement with the calculated value of 17 042.5 cm^{-1}. The EA of ArS is then 2.1129 ± 0.0006 eV. Even though features A–D resemble a vibrational progression, the FC simulation finds very little vibrational activity for the transition between the anion and neutral ground states. Therefore, features B, C, and D must belong to another electronic state of ArS. Based on the FC simulation, these peaks are assigned to the $I1,v \leftarrow X,0$ vibrational states, with $v = 0$, 1, and 2. This assignment yields $T_0(I1) = 31 \pm 5$ cm^{-1} compared to the calculated value of 32.2 cm^{-1}, and $v_0^1 = 24 \pm 5$ cm^{-1} in agreement with the calculated fundamental frequency in Table VI. Features E, F, and G are assigned to the $II0,0 \leftarrow X,0$, $II1,0 \leftarrow X,0$ and $III0,0 \leftarrow X,0$ transitions, respectively, giving the experimental values of $T_0(II0) = 395 \pm 5$ cm^{-1}, $T_0(II1) = 429 \pm 5$ cm^{-1} and $T_0(III0) = 598 \pm 5$ cm^{-1}. The very weak peaks a and b are assigned to the $X2,0 \leftarrow I,0$ transition and the $X2,1 \leftarrow X,1$ sequence band, respectively. The overall pattern of the features is similar to that of the NeS^- spectrum, in that the most intense transitions are from the anion *X* state to the neutral *X*2, *I*1, and *II*0 states. However, the $I1 \leftarrow X$ band exhibits a vibrational progression as opposed to appearing as a single peak. In addition, a weak transition to the neutral *II*1 state is seen in the ArS^- spectrum.

The most intense feature in the KrS^- spectrum, peak A at 17 214 cm^{-1}, is assigned to the $X2,0 \leftarrow X,0$ transition, yielding EA(KrS) = 2.1343 ± 0.0006 eV. The peak position is in good agreement with the calculated value of 17 219.5 cm^{-1}. Peaks B–F appear to be associated with a different electronic band than peak A and are assigned to the vibrational progression $I1,v \leftarrow X,0$, with $v = 0$–4. This assignment yields a fundamental vibrational frequency of 24 ± 5 cm^{-1}, which corresponds to the calculated value for the *I*1 state. Compared to ArS^-, this progression is more extended and obviously associated with a different electronic band than peak A. The experimental $T_0(I1) = 45 \pm 5$ cm^{-1} is within 1 cm^{-1} of the 45.7 cm^{-1} calculated value in Table VII. As in the NeS^- and ArS^- spectra, peak G, lying 396 cm^{-1} above the origin transition, is assigned to the $II0,0 \leftarrow X,0$ transition. The KrS^- SEVI spectrum exhibits more hot band transitions than the NeS^- and ArS^- spectra, a reasonable result given that ion source conditions do not have to be as cold to generate KrS^-. Peaks a, b, c, and d are assigned to transitions from the *II*,0 state to the *X*2,0, *I*1,0, *II*0,0, and *II*1,0 states, respectively. This assignment yields the anionic $T_0(II)$ to be 507 ± 5 cm^{-1}, in agreement with the calculated term energy of 510.3 cm^{-1}. Finally, peaks e and f are assigned to transitions originating from the *I*,0 state to the *X*2,0 and *I*1,0 states, respectively, yielding $T_0(I) = 28 \pm 5$ cm^{-1}, close to the calculated value of 34.1 cm^{-1}.

VI. DISCUSSION

The peak positions in the SEVI spectra are a direct measure of energy differences between the various anion and neutral states of the RgS complexes, while the extent of vibrational activity within each electronic band is most sensitive to the change in bond length between the RgS^- and RgS electronic states involved in the transition. The information

provided by SEVI is thus quite complementary to scattering and ion-mobility experiments that provide absolute values for well depths and bond lengths. However, given the excellent agreement between the experimental SEVI spectra and simulations based on the anion and neutral potential energy curves described in Sec. IV, it is reasonable to assume for the purposes of this discussion that the calculated well depths and bond lengths in Tables V–VII are accurate.

Considering first the overall energetics, the position of the origin transition (or EA) shows a clear blueshifting trend progressing from atomic S^- to NeS^-, ArS^-, and KrS^-. The origin transition for the most weakly bound complex studied here, NeS^-, is shifted by only 46 cm^{-1} from atomic S^-, while ArS^- and KrS^- show much larger shifts of 289 cm^{-1} and 461 cm^{-1}, respectively. These values highlight the large difference in the RgS interactions for Ne as opposed to Ar and Kr. The theoretical results show that for the ground states of NeS^- and NeS, D_0 is only 78.7 cm^{-1} and 34.5 cm^{-1}, respectively, whereas the corresponding values for ArS^- and ArS are 409.1 cm^{-1} and 119.7 cm^{-1}. Dissociation energies for KrS^- and KrS are 629.9 cm^{-1} and 163.4 cm^{-1}. Hence, while the anion and neutral dissociation energies increase with the size of the rare gas atom, this effect is much more dramatic in going from Ne to Ar than from Ar to Kr. To zero order, one can understand this effect in terms of the small Ne polarizability (0.3956 $Å^3$) compared to Ar (1.6411 $Å^3$) or Kr (2.4844 $Å^3$), resulting in a weaker van der Waals attraction and ion-induced dipole interaction in NeS and NeS^-, respectively.

The trends in ground state bond lengths are also noteworthy. The bond length in NeS^- is much longer (3.897 Å) than in neutral NeS (3.596 Å), even though D_0 for the anion is twice the value of the neutral. As the RgS interaction becomes stronger, the difference in the bond length between the anion and the neutral decreases, with ArS^- (3.744 Å) being only slightly longer than the ArS (3.722 Å). This trend is continued in KrS, though to a less dramatic extent, with the anion (3.726 Å) being slightly shorter than the neutral (3.781 Å). These values also show that while the neutral bond length increases with the size of the rare gas atom, the anion bond length decreases, an effect also seen, although far less strikingly, in ArO^- and KrO^-.[24,25] The trend in RgS^- bond lengths can be rationalized by considering the competing charge/induced-dipole and repulsive electron-electron interactions. In NeS^-, the small Ne polarizability insures that the latter dominates at relatively large internuclear distances, leading to a long bond length and relatively little perturbation of the S^- electron cloud by the Ne atom.

The similarity of the spin-orbit fine structure in the SEVI spectrum of S^- and NeS^- provides additional strong evidence for minimal perturbation of both S^- and S upon the addition of a Ne atom. Comparison of the two spectra in Fig. 2 shows that the only observable change in the atomic spin-orbit fine structure is a splitting of the $S(^3P_2)$ state into the NeS $X2$ and $I1$ states (peaks A and B in Fig. 2), which are separated by only 9 cm^{-1}. This splitting increases to 31 cm^{-1} and 45 cm^{-1} in the SEVI spectra of ArS^- and KrS^-, respectively. For all three systems, but especially for NeS^-/NeS, spin-orbit splittings are larger than characteristic electronic interactions as exemplified by the $^2\Sigma^+ - {}^2\Pi$ and $^3\Pi - {}^3\Sigma^-$ splittings (i.e., differences in D_e) in Tables S1–S3. Hence, Hund's case c coupling is most appropriate for describing the anion and neutral complexes.

The ArS^- and KrS^- spectra show no vibrational activity in the $X2$-X band but extended progressions in the $I1$-X band. These results are readily explained by the small change in bond length upon photodetachment to the $X2$ state and the considerably larger change upon photodetachment to the $I1$ state: +0.219 Å for ArS^- and +0.301 Å for KrS^-, according to the calculated curves in Tables VI and VII. We note that in ArO^- and KrO^-, bond length changes are considerably larger for photodetachment to the neutral $X2$ and $I1$ states,[24,25] to the extent that vertical photodetachment accesses the repulsive wall of both neutral states. This results in considerable overlap with neutral continuum wavefunctions and a broad feature underneath the sharp peaks in the SEVI spectra of ArO^- and KrO^-. This broad feature is absent in the RgS^- spectra since photodetachment leads to much better overlap with the neutral bound states.

In contrast, no vibrational progressions are seen in the NeS^- spectrum. This result is somewhat surprising given that the calculated potentials in Table V show a significant decrease in bond length, −0.301 Å, upon photodetachment to the $X2$ state of NeS. The absence of a progression reflects the very shallow and anharmonic nature of the NeS neutral potential energy curves, each of which can only support three vibrational levels. The wavefunctions for the neutral excited vibrational levels are very diffuse and mostly located at larger bond distance, resulting in poor overlap with the anion ground state wavefunction.

VII. CONCLUSION

The high-resolution photoelectron spectra of RgS^- (Rg = Ne, Ar, and Kr) obtained using the slow electron velocity-map imaging technique are reported. Fully resolved vibrational, electronic, and spin-orbit structure is seen for all three species. High level *ab initio* calculations on the RgS^- and RgS are presented and used to simulate the SEVI spectrum. Several RgS^- and RgS vibrational frequencies and excited-state term energies are accurately determined from the analysis of the experimental spectra and are found to be in excellent agreement with the calculated values. The electronic and vibrational structures revealed by these spectra changes markedly with the identity of the rare gas atom. The NeS^- spectrum is very similar to that of bare S^-, while the SEVI spectra of ArS^- and KrS^- are more characteristic of diatomic molecules.

ACKNOWLEDGMENTS

This work was supported by the Air Force Office of Scientific Research (AFOSR) under Grant Nos. F49620-03-1-0085 and FA9550-09-1-0343. E.G. thanks the National Science and Engineering Research Council of Canada (NSERC) for a post graduate scholarship.

[1] A. D. Buckingham, P. W. Fowler, and J. M. Hutson, Chem. Rev. **88**(6), 963 (1988).
[2] K. Müller-Dethlefs and P. Hobza, Chem. Rev. **100**(1), 143 (1999).

[3]E. A. Meyer, R. K. Castellano, and F. Diederich, Angew. Chem. Int. Ed. **42**(11), 1210 (2003).
[4]J. J. Gilijamse, S. Hoekstra, S. Y. T. van de Meerakker, G. C. Groenenboom, and G. Meijer, Science **313**(5793), 1617 (2006).
[5]D. D. Nelson, G. T. Fraser, and W. Klemperer, Science **238**(4834), 1670 (1987).
[6]K. Liu, J. D. Cruzan, and R. J. Saykally, Science **271**(5251), 929 (1996).
[7]P. E. S. Wormer and A. van der Avoird, Chem. Rev. **100**(11), 4109 (2000).
[8]W. H. Robertson and M. A. Johnson, Annu. Rev. Phys. Chem. **54**, 173 (2003).
[9]M. L. Dubernet, D. Flower, and J. M. Hutson, J. Chem. Phys. **94**(12), 7602 (1991).
[10]M. C. Heaven, Annu. Rev. Phys. Chem. **43**, 283 (1992).
[11]C. H. Becker, P. Casavecchia, and Y. T. Lee, J. Chem. Phys. **69**(6), 2377 (1978).
[12]C. H. Becker, P. Casavecchia, and Y. T. Lee, J. Chem. Phys. **70**(6), 2986 (1979).
[13]V. Aquilanti, E. Luzzatti, F. Pirani, and G. G. Volpi, J. Chem. Phys. **89**(10), 6165 (1988).
[14]V. Aquilanti, R. Candori, and F. Pirani, J. Chem. Phys. **89**(10), 6157 (1988).
[15]D. M. Neumark, J. Chem. Phys. **125**, 132303 (2006).
[16]T. N. Kitsopoulos, I. M. Waller, J. G. Loeser, and D. M. Neumark, Chem. Phys. Lett. **159**(4), 300 (1989).
[17]Y. X. Zhao, I. Yourshaw, G. Reiser, C. C. Arnold, and D. M. Neumark, J. Chem. Phys. **101**(8), 6538 (1994).
[18]I. Yourshaw, T. Lenzer, G. Reiser, and D. M. Neumark, J. Chem. Phys. **109**(13), 5247 (1998).
[19]T. Lenzer, I. Yourshaw, M. R. Furlanetto, G. Reiser, and D. M. Neumark, J. Chem. Phys. **110**(19), 9578 (1999).
[20]T. Lenzer, I. Yourshaw, M. R. Furlanetto, N. L. Pivonka, and D. M. Neumark, J. Chem. Phys. **116**(10), 4170 (2002).
[21]A. Osterwalder, M. J. Nee, J. Zhou, and D. M. Neumark, J. Chem. Phys. **121**(13), 6317 (2004).
[22]D. M. Neumark, J. Phys. Chem. A **112**(51), 13287 (2008).
[23]E. Garand, J. Zhou, D. E. Manolopoulos, M. H. Alexander, and D. M. Neumark, Science **319**(5859), 72 (2008).
[24]E. Garand, A. A. Buchachenko, T. I. Yacovitch, M. M. Szcześniak, G. Chałasiński, and D. M. Neumark, J. Phys. Chem. A **113**, 4631 (2009).
[25]E. Garand, A. A. Buchachenko, T. I. Yacovitch, M. M. Szczesniak, G. Chalasinski, and D. M. Neumark, J. Phys. Chem. A **113**(52), 14439 (2009).
[26]C. C. Kirkpatrick and L. A. Viehland, Chem. Phys. **98**(2), 221 (1985).
[27]L. A. Viehland, R. Webb, E. P. F. Lee, and T. G. Wright, J. Chem. Phys. **122**(11), 114302 (2005).
[28]H. L. de Clercq, J. H. Hendricks, and K. H. Bowen, J. Chem. Phys. **117**(6), 2619 (2002).
[29]V. Aquilanti, D. Ascenzi, E. Braca, D. Cappelletti, and F. Pirani, Phys. Chem. Chem. Phys. **2**(18), 4081 (2000).
[30]J. Klos, G. Chalasinski, R. V. Krems, A. A. Buchachenko, V. Aquilanti, F. Pirani, and D. Cappelletti, J. Chem. Phys. **116**(21), 9269 (2002).
[31]M. B. Sevryuk, L. Y. Rusin, S. Cavalli, and V. Aquilanti, J. Phys. Chem. A **108**(41), 8731 (2004).
[32]T. G. Wright and L. A. Viehland, Chem. Phys. Lett. **420**(1–3), 24 (2006).
[33]A. Eppink and D. H. Parker, Rev. Sci. Instrum. **68**(9), 3477 (1997).
[34]U. Even, J. Jortner, D. Noy, N. Lavie, and C. Cossart-Magos, J. Chem. Phys. **112**(18), 8068 (2000).
[35]W. C. Wiley and I. H. McLaren, Rev. Sci. Instrum. **26**(12), 1150 (1955).
[36]D. W. Chandler and P. L. Houston, J. Chem. Phys. **87**(2), 1445 (1987).
[37]C. Blondel, W. Chaibi, C. Delsart, and C. Drag, J. Phys. B **39**(6), 1409 (2006).
[38]W. C. Martin, R. Zalubas, and A. Musgrove, J. Phys. Chem. Ref. Data **19**(4), 821 (1990).
[39]H. Hotop and W. C. Lineberger, J. Phys. Chem. Ref. Data **14**(3), 731 (1985).
[40]MOLPRO, a package of *ab initio* programs designed by H.-J. Werner and P. J. Knowles, version 2009.1, R. D. Amos, A. Bernhardsson, A. Berning, *et al.*; see http://www.molpro.net.
[41]A. A. Buchachenko, J. Jakowski, G. Chalasinski, M. M. Szczesniak, and S. M. Cybulski, J. Chem. Phys. **112**(13), 5852 (2000).
[42]A. A. Buchachenko, M. M. Szczesniak, and G. Chalasinski, Chem. Phys. Lett. **347**(4–6), 415 (2001).
[43]A. A. Buchachenko, M. M. Szczesniak, J. Klos, and G. Chalasinski, J. Chem. Phys. **117**(6), 2629 (2002).
[44]P. J. Knowles, C. Hampel, and H. J. Werner, J. Chem. Phys. **99**(7), 5219 (1993).
[45]P. J. Knowles, C. Hampel, and H. J. Werner, J. Chem. Phys. **112**(6), 3106 (2000).
[46]D. E. Woon and T. H. Dunning, J. Chem. Phys. **98**(2), 1358 (1993).
[47]S. F. Boys and F. Bernardi, Mol. Phys. **19**(4), 553 (1970).
[48]C. Puzzarini, J. Phys. Chem. A **113**(52), 14530 (2009).
[49]M. Reiher and A. Wolf, J. Chem. Phys. **121**(22), 10945 (2004).
[50]M. Reiher and A. Wolf, J. Chem. Phys. **121**(5), 2037 (2004).
[51]A. Wolf, M. Reiher, and B. A. Hess, J. Chem. Phys. **117**(20), 9215 (2002).
[52]N. J. DeYonker, K. A. Peterson, and A. K. Wilson, J. Phys. Chem. A **111**, 11383 (2007).
[53]See supplementary material at http://dx.doi.org/10.1063/1.3605595 for the *ab initio* data and the Murrell-Sorbie fitting parameters for the *ab initio* AE-CCSD(T)/CBS-DK and spin-orbit coupled potential energy curves.
[54]J. N. Murrell, S. Carter, S. C. Farantos, P. Huxley, and J. C. Varandas, *Molecular Potential Energy Functions* (John Wiley & Sons, Chichester, 1984).
[55]R. V. Krems and A. A. Buchachenko, J. Phys. B **33**(21), 4551 (2000).
[56]Z. Ma, K. Liu, L. B. Harding, M. Komotos, and G. C. Schatz, J. Chem. Phys. **100**(11), 8026 (1994).
[57]V. Aquilanti, G. Liuti, F. Pirani, and F. Vecchiocattivi, J. Chem. Soc. Faraday Trans. II **85**, 955 (1989).